A power-efficient approach to fiber noise cancellation and normal modes of motion of an isospaced ion string

Alexandra Mestre Torà

Supervised by: Dr. Matteo Marinelli

Spring Semester 2021

Abstract

In the first part of this report we present a power-efficient approach to Fiber Noise Cancellation (FNC) based on the assumption that the phase noise of close and identical fibers is common to all of them. We validate the assumption by cancelling the noise in various fiber paths by locking only one of them. In addition, we also build and test an all in-fiber FNC setup for a compact way of stable light delivery.

In the second part, we calculate the modes of motion of a long chain of ions using the package IonSim. Particularly, we focus on an isospaced potential that keeps all ions equally spaced. We calculate how its normal modes are affected when the analytical potential is replaced by its sixth order polynomial approximation and when using mixed-species.

Contents

Part I

Scaling Fiber Noise Cancellation

1 Introduction

Aiming to push the number of ions in a trap and scale experiments up, one of the key ingredients in quantum systems based on trapped ion technology is the individual control of multiple qubits. Laser light, used for coherent control and manipulation, is a key component of ion trap experiments. In this regard, laser delivery is one of the main challenges that has to be addressed. The desired setup should be compact, robust and present reduced losses. At the same time should allow individual manipulation of qubits.

For driving a transition in a qubit defined on the quadrapole transition of a $^{40}Ca^{+}$ ion, very narrow resonant light at 729 nm is needed. To deliver these laser beams to the vicinity of the ion trap, usually optical fibers are used. Being a very versatile alternative that not only allows the separation of the trapping experiment from the laser setup but also offers compactness, efficiency and scalability, optical fibers come at the expense of a loss of the laser's original frequency stability due to phase noise [1]. This noise is in the kHz range.

Fiber noise cancellation (FNC) in free space is an effective and widely used approach to compensate for phase noise. However, this approach presents some constraints. One of them is that conventional FNC setups are usually not very compact since their minimum sizes are constricted by the space needed to separate and properly align the different orders diffracted by an Acousto-optic modulator (AOM), one of its main building components. Also, if one wishes to cancel noise in more than one fiber component, daisy chaining is required and this makes the process very inefficient in terms of power. Moreover, a continuous beatnote signal is required to continuously suppress the noise. This makes this approach unsuitable for the pulsed light required to address qubits. Summing up, when using more ions and scaling up, having one FNC setup for each fiber is not the most suitable alternative in terms of space, power and convenience.

In this part of the work, we first propose and test an alternative power-effcient approach to FNC that is based on the assumption that signals propagating through identical fibers sitting closeby experience the same phase noise. We also build and test an all in-fiber FNC experiment that allows for even a more compact setup.

2 Fiber noise cancellation

2.1 Theoretical Background

2.1.1 Phase noise in optical fibers

The transmission of frequency-stabilized laser light through optical fibers is a practical and easy way to transmit and distribute light to various locations. Attractive because their flexibility and robustness, optical fibers have the disadvantage that light propagating through them likely experience a broadening of the linewidth due to phase noise. This noise has origin in the random fluctuations of the optical path length in the fiber that are induced by acoustic effects such as thermal or mechanical variations [2]. Being most of the time a harmful phenomenon, the high sensitivity to environmental changes can in fact be used for sensing purposes [3].

When propagating through a medium, a phase ϕ proportional to the optical phase length (OPL) is added to the light field. In an idealized situation in which the refractive index of the propagating homogeneous material n, as well as the exact length of the path that light travels γ are stable, the OPL is simply given by:

$$\mathrm{OPL} = \int_\gamma n(\vec{r})d\vec{r} = n\,|\gamma| \tag{1}$$

However, for real-world applications, the medium of propagation is not perfectly homogeneous and stable. Acoustic waves that generate pressure waves inside the fiber [4] or thermal effects [5] produce fluctuations in the refractive index, in the path length and ultimately in the OPL. This results in a stochastic modulation of the phase shift that leads to a broadening of the linewidth of the stabilized laser. All these effects scale with the length of the fiber.

Phase noise effects have been studied and characterized for several decades. For example, acoustic waves from a normal-speech can produce a frequency broadening of ~ 1 KHz [1] (from several Hz to a few kHz).

2.1.2 Classical Fiber Noise Cancellation

Different stabilization techniques have been proposed for cancelling phase noise and successfully deliver very stable laser light. The approaches are usually based on a locking stabilization scheme with a double-passed AOM. The scheme was firstly proposed and implemented in [2].

The method underlies in two assumptions. The first one is that the phase noise induced by the fiber is linear and reciprocal, implying that two counterpropagating paths propagating at the same time t experience the same phase shift $\phi_f(t)$. The second is that the phase noise fluctuations or $\dot{\phi_f}(t)$ are slow with respect to the bandwidth of the locking electronics.

The basic setup is shown in Figure 1 and a more detailed description and mathematical derivation that what is presented here can be found in [6].

The main idea is to use the phase shift ϕ_{AOM} induced by the AOM, that is driven by a VCO at frequency Δ, to actively compensate for the noise introduced by the optical fiber. For that, the -1st order reflection from the AOM is directed to a PC-ended fiber used for light delivery that adds a phase noise of ϕ_f. In this fiber around 4% of the light is reflected back. Passing twice through it, the reflected signal acquires a phase $2\phi_f + \phi_{\mathrm{AOM}}$. For the first 0th order, it is back-reflected to the AOM and the +1st order emerging from it is made interfere with the 0th order coming from the reflected +1st order. Bearing in mind that the $\pm$1st orders are also shifted $\pm\Delta$ in frequency, the interference produces a beat note that oscillates as:

$$\cos\left(\Delta t + \phi_{\mathrm{AOM}} - \phi_t\right) \cdot \cos\left(\Omega t\right) \tag{2}$$

This interference is detected by an AC photodiode. The fast oscillation at an optical frequency falls outside the bandwith of the detector and only the RF component is measured. The intensity of this beat note is at 2Δ (because $I = |E|^2 \propto \cos^2(\times) \propto \cos(2\times)$). The RF-signal is mixed down to DC by a frequency mixer that takes a stable reference source at a frequency close to 2Δ as the local oscillator (LO). A low-pass filter eliminates the RF component at approximately 4Δ so as to end up with a DC signal containing the two phases $\phi_f - \phi_{\mathrm{AOM}}$. This is the error signal that is then sent to a feedback loop that controls the driving frequency of the AOM. This control system is known as a phase-locked loop (PLL). [7] provides an extensive review of the theory behind it.

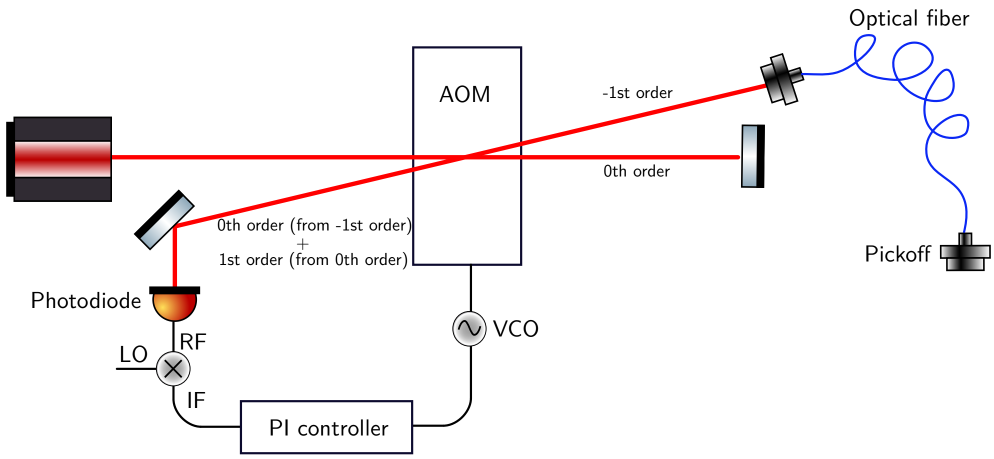

Figure 1: Experimental setup for the conventional FNC. The different orders diffracted by the AOM produce a beatnote at around the driving frequency of the AOM. The beatnote contains the noise induced by the fiber and with a PLL it is possible to drive the AOM at the right modulation frequency to compensate for the noise.

2.2 Optical and electronic components

In this section we describe the operation principle of the main elements present in the test setups we built in this project.

2.2.1 FAOM

A Fiber-Coupled Acousto-Optic Modulator (FAOM) is a device used to modulate the amplitude and phase of light propagating through fibers, avoiding having to launch it to free-space. FAOMs are compact, practical and versatile devices that do not require any external alignment.

A FAOM has two reciprocal fiber ports that couple light into a compact-packaged optical assembly. The housing contins two fiber collimators and two aspheric lenses that align the light to an AOM (a description of it is given in the section that follows). The alignment is such that the AOM operates in the Bragg regime and the coupling efficiency to the +1st order is maximized. The transducer of the AOM is impedance-matched to an RF input through an SMA cable. Figure 2 shows a detailed drawing of the interior of the device.

The Acusto-Optic Modulator

An acousto-optic modulator (AOM) is a device used to frequency-shift, modulate the intensity and diffract an incoming light beam based on the acousto-optic effect. The device typically consists of an acousto-optic cell, usually a transparent crystal, attached to a piezoelectric transducer electrically driven at RF frequencies [9]. The transducer generates acoustic waves inside the cell that in turn produce a periodic modulation of its refractive index through the photoelastic effect. This travelling gradient of the refractive index Bragg-diffracts the incoming light producing a frequency shift and modulating the intensity.

The frequency of the driving determines the diffraction angle and the frequency shift whereas the driving amplitude controls the diffracted power. AOMs can be operated in the Raman-Nath

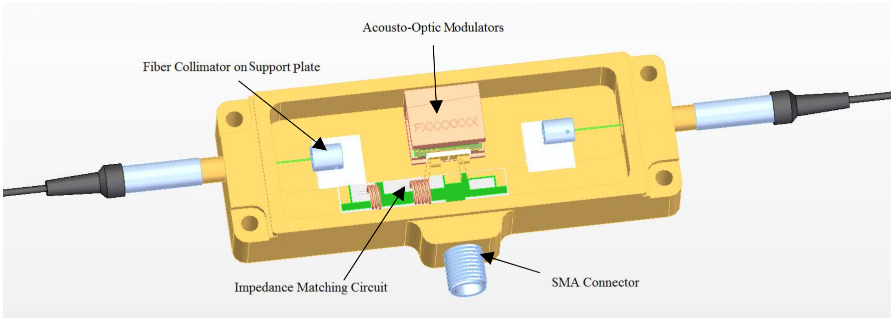

Figure 2: Interior of a FAOM. Fiber collimators focus the light into the AOM with the right alignment to operate in the Bragg regime and to maximize the coupling to the +1st diffraction order. Extracted from [8].

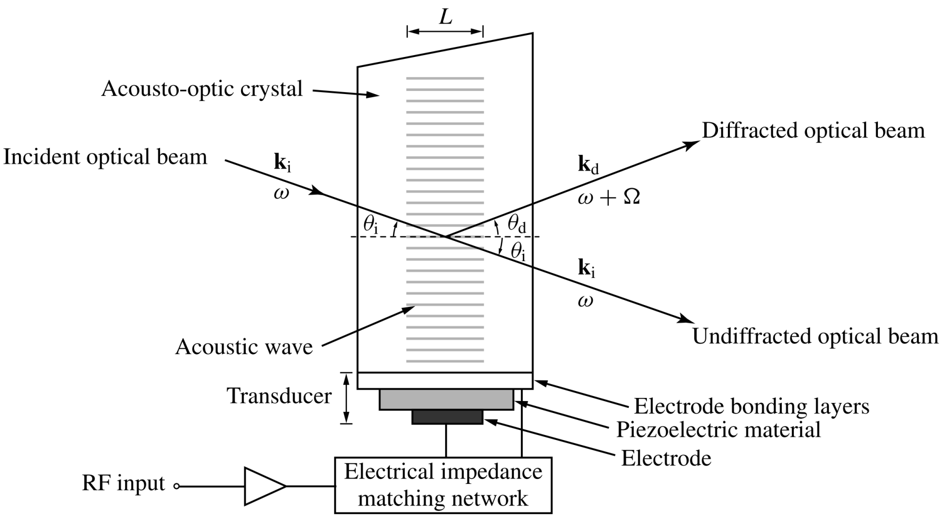

Figure 3: Acusto-optic modulator operated in the Bragg regime. Light at frequency ω is incident at a Bragg angle θ_i to a acusto-optical crystal driven at Ω. The beam is mainly difre

or in the Bragg regime. In the Raman-Nath regime, light is normally incident to the AOM and several diffracted beams are produced. In the Bragg regime, light has to be incident at a particular angle called the Bragg angle and just one diffraction (the +1st order) is produced.

2.2.2 POISON

The POISON board is a PCB containing two separate circuits. The first one is a phase-error detector circuit. It mixes down to DC the AC input signal from the photodiode using a frequency mixer. An operational amplifier in the IF (intermediate frequency) port filters out the high-frequency components of the mixing with the LO stable source. In our implementation we use AWG Aimtti TGF4242 and Rohde & Schwarz SMC100A as stable sources in the LO port. The second circuit is a low-noise circuit that drives the VCO at the right frequency and amplitude with the aim to compensate for the phase-error detected. Moreover, the POISON board has another feedback circuit for suppressing intensity noise.

2.2.3 EVIL

The Electronically Variable Interactive Lock-box or EVIL is a digital FPGA-based PI-Controller developed and improved in [10, 11]. It is used as a PI controller in the multiple stabilization loops in the laboratory that for example do Pound–Drever–Hall, beatnote or intensity locking. The fast channel has a control bandwidth of $\sim$ 500 kHz, large enough for our setup where slower fluctuations due to acoustic noise (always lower than 100 kHz) are expected.

2.2.4 Optical circulator

An optical circulator, the optical analogous of an electric circulator, is a nonreciprocal device (its properties depend on the direction of propagation) used to separate counter-propagating beams in optical fibers. Though there exist multiple different designs for a circulator, almost all of them include similar components: polarizing beam splitters, Faraday rotators and some of them also birefringent crystals that walk off different propagation directions. The operational principle of the optical circulator is quite similar to the optical isolator but each design uses a slight different approach. Figure 4 shows and describes one of the simplest implementations of a 3-terminal circulator.

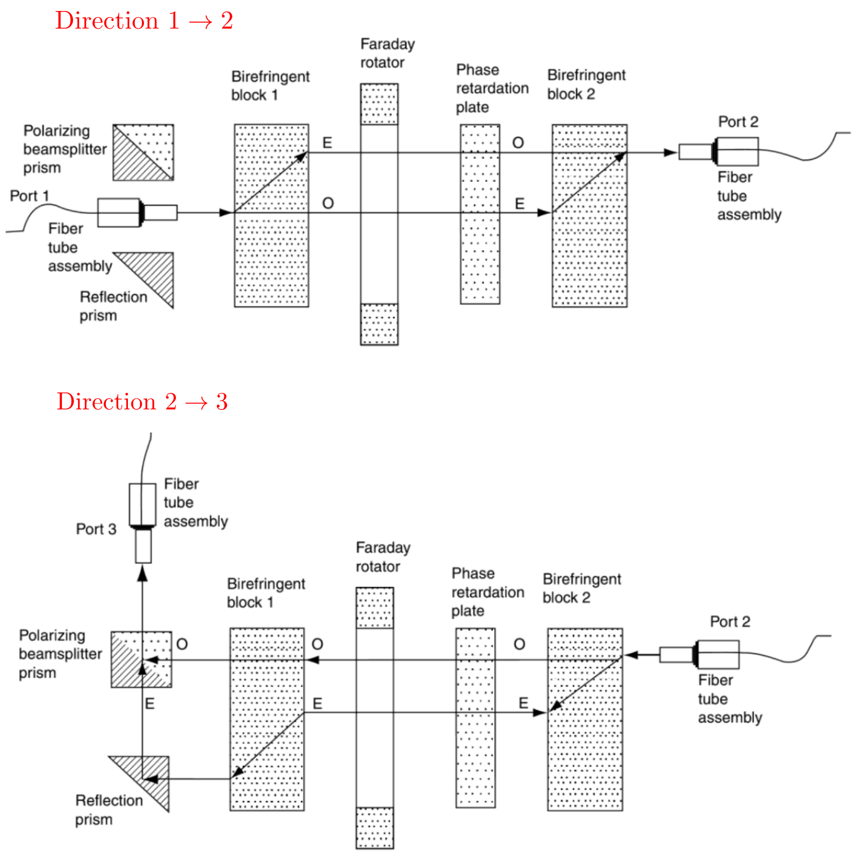

Figure 4: Operating principle of an optical circulator. $1 \to 2$ direction: a birefringent glass walks off two orthogonal polarizations and the combination of the Faraday rotator and the phase-retarder plate rotates the polarization vector by $90°$, finally the rays recombine in a second birefringent glass and couple into Port 2. $2 \to 3$ direction: after the separation by polarization, the Faraday rotator and the waveplate rotate the polarization vector in opposite directions giving rise to a zero net rotation. After passing the first birefringent block, the rays meet up in a PBS and are coupled into Port 3.

3 Experimental setup

3.1 Scalabe single-pass FNC

3.1.1 Setup and principle

In this part we present the optical and electronic setup built to perform power-efficient FNC. In a nutshell, the main idea is to use several identical fiber links and to place them in a compact and symmetric way so that they are exposed to the same acoustic noise mechanisms. Then one of the links (in-loop) is used to detect the phase noise and to cancel it with a feedback loop. The same feedback is also applied to the other fibers (out-of-loop), suppressing also the noise in them. This validates the hypothesis of common noise in close and identical fibers. The full schematics is shown in Figure 5.

A 729 nm stable light beam oscillating at Ω_L is launched from an optical fiber to free space. Right after, a half-wave plate followed by a polarizing beam splitter are used to separate the

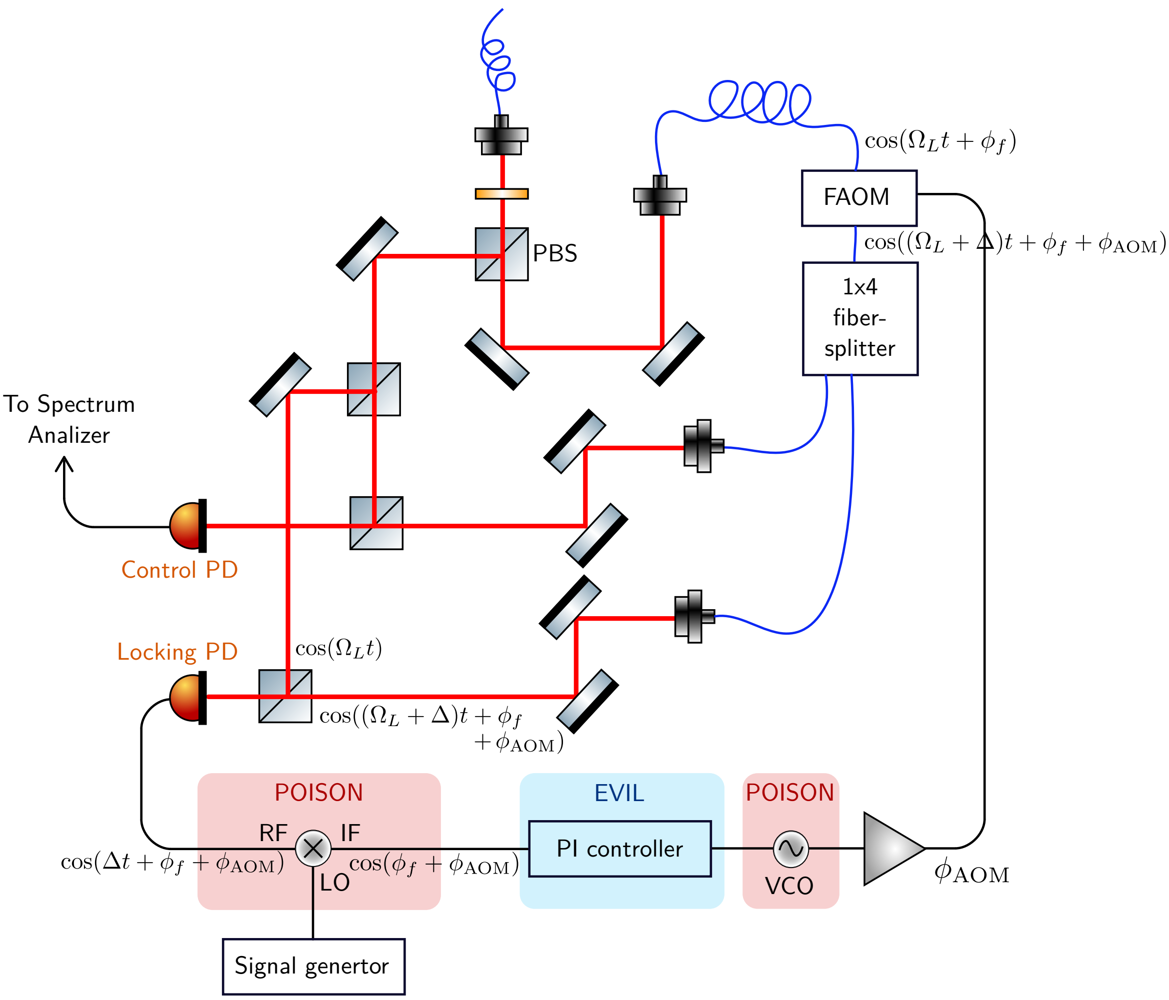

Figure 5: Experimental setup for the scalable FNC.

light into two beams. The reflected light serves as the clean and narrow reference and is used to produce the beat note at a latter stage. The transmitted beam is coupled back to a long fiber and will eventually be subject to acoustic noise. To resemble a more realistic fiber link, we use an 8 m long 630HP single mode fiber. When passing through the fiber, light gains a time-dependent phase $\phi_f(t) \equiv \phi_f$. The output is sent into a FAOM that is driven by the VCO in the POISON board at a frequency Δ, around 150 MHz. One of the differences with respect the conventional FNC approaches is that in this case the FAOM is not double-passed. The FAOM shifts the frequency by Δ and adds a phase-shift of $\phi_{\rm AOM}$. As a result, after the FAOM and the fiber the field oscillates with the $\cos\left((\Omega_L + \Delta)t + \phi_f + \phi_{\rm AOM}\right)$.

At this stage the light is split into four beams with a 1x4 fiber optic coupler from Thorlabs (model TWQ850HA) and two of the four outputs are launched to free space again. A beat note is created by interfeering them with the narrow linewidth light reflected in the first beamsplitter and that was not coupled again to a fiber. The beating is detected with a silicon photodetector from Electro-Optics (model ET-2030).

The intensity of the field impinging the photodiode is:

$$I = |A_1 \cos((\Omega_L + \Delta)t + \phi_f + \phi_{\mathrm{AOM}}) + A_2 \cos(\Omega_L t)|^2 = I_1 + I_2 + I_3 \tag{3}$$

Using trigonometric identities for the cosinus, we find that each of the contributions oscillates as:

$$\begin{gathered} I_1 \propto \cos^2((\Omega_L + \Delta)t + \phi_f + \phi_{\mathrm{AOM}}) \propto \cos(2(\Omega_L + \Delta)t + 2\phi_f + 2\phi_{\mathrm{AOM}}) \\ I_2 \propto \cos^2(\Omega_L t) \propto \cos(2\Omega_L t) \\ I_3 \propto \cos((\Omega_L + \Delta)t + \phi_f + \phi_{\mathrm{AOM}}) \cos(\Omega_L t) \propto \\ \cos((2\Omega_L + \Delta)t + \phi_f + \phi_{\mathrm{AOM}}) + \cos(\Delta t + \phi_f + \phi_{\mathrm{AOM}}) \end{gathered}$$

The addition of I_1 and I_2 results in a fast oscillation at $2\Omega_L$ modulated with the $\cos(\Delta t + \phi_f + \phi_{\mathrm{AOM}})$. One of the terms in I_3 are also fast oscillating at $2\Omega_L$ while the other also comes with the $\cos(\Delta t + \phi_f + \phi_{\mathrm{AOM}})$. Because the carrier frequency Ω_L is in the THz range, it is completely spectrally separated from the oscillation at Δ, in the RF range. The photodiode, with a bandwidth extending up to few GHz, acts as a filter for these frequencies and the main contribution of the photodetected current is the the beat note at Δ. This RF signal is sent to a frequency mixer in a POISON board where is mixed down to DC using a stable reference source (AWG Aimtti TGF4242 or Rohde & Schwarz SMC100A). The resulting DC signal carries the information about the phase noise and it is the error input to the PI-Controller in the EVIL board. The controller outputs the correcting voltage so that the VCO drives the FAOM at the appropriate frequency to eliminate the contribution of ϕ_f.

3.1.2 Characterization of the Fiber-AOM

The fiber-coupled AOM used is a 780 nm FAOM from Gooch & Housego (model T-M150-0.5C2W-3-F2S) with a nominal insertion loss of 3 dB and a polarization dependent loss of 0.5 dB. The device has to be driven with an RF signal of 150 MHz with a power up to 1 W. The amplitude of the output of the AWG (Aimtti TGF4242) used to generate the RF signal is adjusted so that after the amplification stage there is 1 W. For the amplification, a 27 dB amplifier from Minicircuits (model 3ZHL3AS+) is used. We measure the transmission of the FAOM for a range of frequencies around 150 MHz and also explore different drive powers. As seen in Figure 6, the maximum transmission is 35.8% (which corresponds to an attenuation of 4.45 dB) when the driving it at 150 MHz and the signal before amplification is 700 $\mathrm{mV_{PP}}$ (or 28 dBm after amplification). The measured insertion losses also take into account coupling losses and there can also be some olarization sensitivity.

3.1.3 Beat note signals

The beat note signals detected at the photodiodes are measured with an spectrum analyzer. By examining the beat note and its properties we will characterize the phase noise of the setup and its performance in cancelling phase noise.

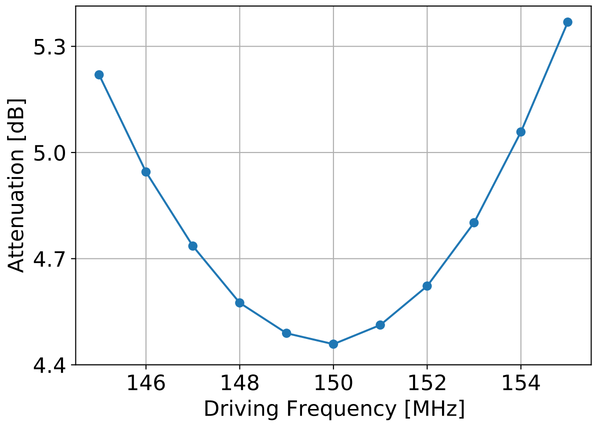

Figure 6: Attenuation of the FAOM for driving frequencies around 150 MHz.

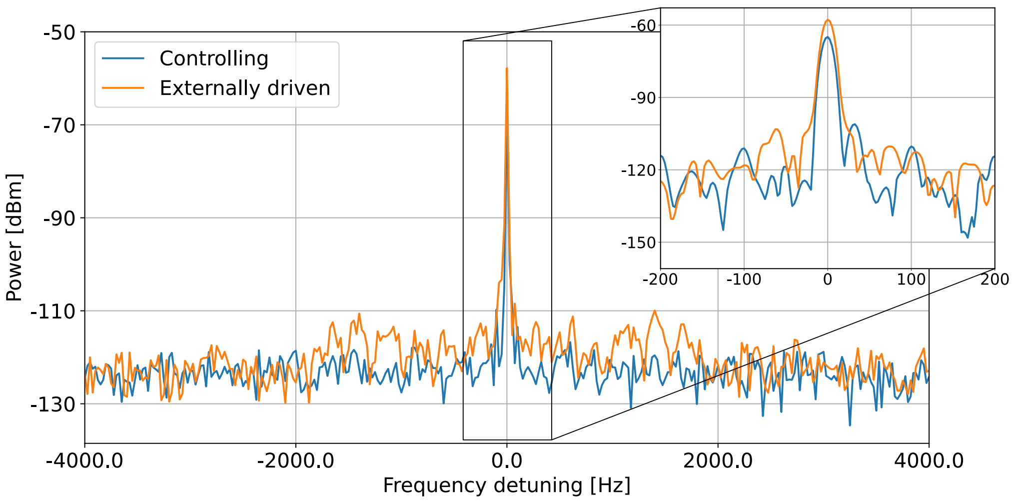

Figure 7: Beat note measurement of the in-loop photodiode when driving the FAOM directly with the AWG (orange spectrum, centered at 150.00006 MHz) and when the feedback loop is used (blue spectrum, centered at 149.99997 MHz). When not locked, the beatnote is slightly wider (see inset) and a noise pedestal of ~ 4 kHz appears.

Figure 7 shows the unlocked (orange) and locked (blue) beat note spectra of the in-loop photodiode. The unlocked beat note is centered at 150.00006 MHz and is obtained by directly driving the FAOM with the reference source (Rohde & Schwarz SMC100A), without using the electronic boards. When the fibers are left untouched, the beat note is very narrow in linewidth with a broadening of 31 Hz (FWHM of a Lorentzian fitting) and a pedestal due to phase noise of ~ 4 KHz, roughly 10 dB above the noise floor. Moreover, any small movement or vibration of the fiber completely destroys the stability of the beat note and broads it a few kHz. Regarding the locked beat note, a slightly more narrow peak at 149.99997 MHz is achieved by properly adjusting the locking parameters. The fitted linewidth at FWHM is of 32 Hz. By locking, the acoustic noise is effectively suppressed and the beat note becomes more robust to gentle vibrations. In the inset plot we also observe a small peak to the right of the locked beat note, this is a back-reflected signal from the electronics. These two traces were collected with the finest resolution (10Hz) of the spectrum analyzer. Being the signals quite narrow, probably a spectrum analyzer with higher resolution (up to 1Hz) could have provided more resolved data for a richer analysis. It is important to note that for a fair analysis of the noise induced by the fiber, the FAOM has to be driven with a stable reference source and not with the VCO. Otherwise, the noise added by the free running VCO broads the beat note a few kHz and totally hides the acoustic noise because of the fiber.

From the plot, we can also conclude that the fiber we used (630 HP single mode) doesn't add much noise: the beat note is just broadened a few Hz and the acoustic noise is very week in power. Something that could be worth discussing is the effective impact in the experiment of this noise and what detunnings and power levels can be tolerated. For that Monte Carlo simulations would be needed and this falls out of the scope of this project.

Two paths comparison

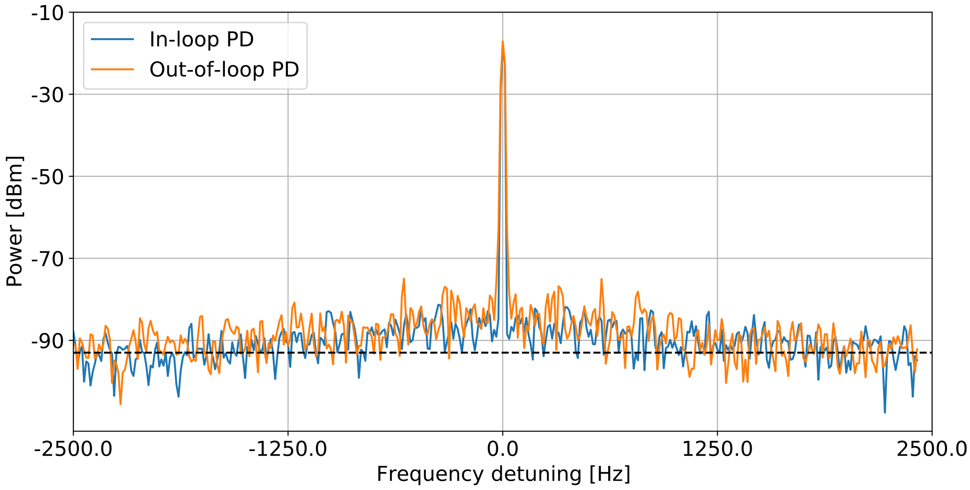

Figure 8: Beat note in the in-loop (locked) and in the out-of-loop photodiodes. The two peaks are centered at 150.00001 MHz and have almost the same linewidth. Some phase noise appears in the two signals and probably inherited from the AWG. The out-of-loop trace, that is not directly locked, is a little bit more noisy.

The next step was to verify the assumption of the common noise. For that we split the light into two paths: an in-loop path that was beat-locked (Locking PD in Figure 5) and an out-of-loop that was not (Control PD in Figure 5). Both fibers were identical and were placed close enough so that hypothetically the noise was common: any noise added to one fiber was also added to the other one. Being this the case, the locking for the in-loop fiber would also suppress the noise in the out-of-loop one.

The beat notes in the in-loop and in the out-of-loop photodiodes are shown in Figure 8 and both of them are centered at 150.00001 MHz. The difference in the alignment of the two detectors resulted in a slightly less powerful signal at the out-of-loop photodiode. To help in the analysis, the noise floor of the spectra were matched by shifting up 3 dB the in-loop trace. Also, a black dashed line was plotted as a reference for the noise floor.

The first observation is that the beat notes are very simmilar and have a very narrow linewidth. This indicates that either there is no much noise added or that the noise in the two paths is common. Nonetheless, the out-of-loop spectrum does look a bit more noisy. This is expected because this path is not directly noise-cancelled as a whole but the portion after splitting is noise-cancelled indirectly.

Besides and in contrast to what was seen in 7, the two beat notes show a slight widening of a few dBm around the carrier frequency, between around ± 1.2kHz. The effect is slightly more noticeable in the out-of-loop signal, probably because of its more noisy nature explained above. Our main hypothesis, to be contrasted, is that the widening comes from using the Aimtti AWG instead of the Rohde & Schwarz one. We suspect that the widening probably comes from the intrinsic phase noise of the Aimtti AWG. Other sources of origin could be a non-proper adjustment of the control parameters or the fiber splitter not used for the previous measurements. Also, not having identical experimental conditions for the two measurements could also play some role since the spectra were taken with modified setups and in different days.

Modification of the out-of-loop path

Figure 9 shows the beat notes at the out-of-loop photodiode with different modifications of the out-of-loop path. The *Direct* trace corresponds to the unaltered setup in which after splitting, light goes through the same fiber used for the in-loop path in the previous section. The *+FAOM* and *+Fiber* refer to the addition of an extra FAOM or a fiber in the second path. This alters the symmetry of the paths (by changing the path length in the out-of-loop path or also adding an extra element) and therefore the possibility of uncorrectable differential fiber phase noise is increased. The addition of any of the two extra elements only results in a noticeable decrease of the detected power (11dB for the FAOM and 28dB for the fiber). Surprisingly enough, we didn't observe any differential noise in the kHz range. This is an unexpected result that seems to indicate that not the FAOM nor the fiber add too much phase noise.

Regardless, there are few considerations that is worth making. The first one is that so as to compensate for the power difference the traces were shifted to make the noise floors coincide. Also, the range of the measured spectra, however, might not be large enough to capture the real noise floor and do a right compensation. For future measurements, the width of the spectra should be larger, at least 10 kHz wide so as to make sure that the baselines don't have any noise contribution at all. Another thing that we notice is that the broadband noise around the carrier previously observed is also seen here, we also suspect that this is because of the Aimitti AWG. Moreover, there are also some additional side peaks separated some hundreds of Hz from the carrier frequency, those are due to electronics.

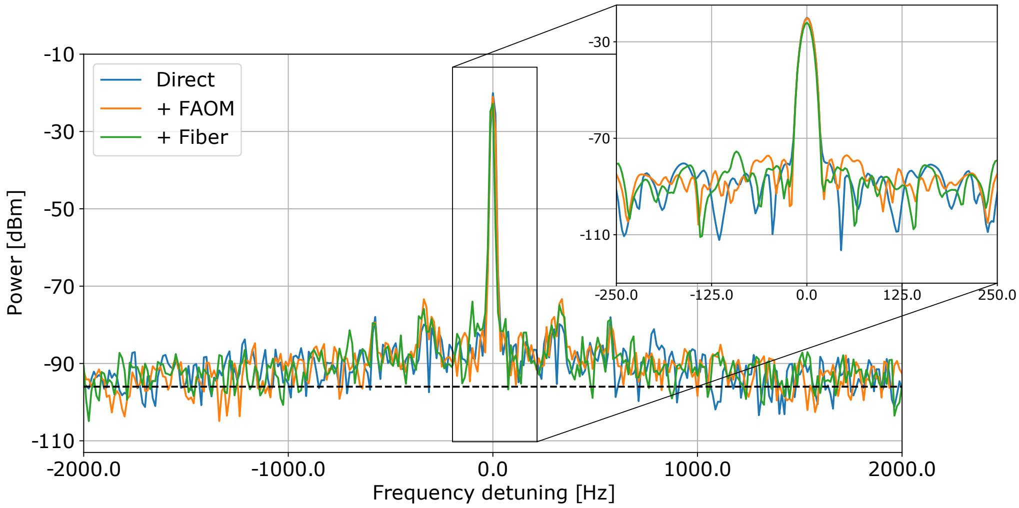

Figure 9: Beat note in the out-of-loop photodiode for different modifications of the out-of-loop path while the in-loop path is being stabilized. The blue trace (*Direct*) corresponds to the unmodified path whereas for the orange (+ *FAOM*) and the green (+ *Fiber*) traces an extra FAOM or a 8m fiber where added before generating the beat note, making the in-loop and out-of-loop paths asymmetrical. The beat notes are centered at 150.00009 MHz, 300.00019 MHz and 150.00009 MHz respectively. The addition of extra FAOM or fiber produces a significant power loss. For a better comparison, all spectra are matched to have the same noise floor. For that, the + *FAOM* is shifted 11 dB and + *Fiber* 28 dB.

3.2 All in-fiber FNC

Inspired by the conventional FNC setups, we adapted the free-space approach to a version in which everything except for the beat note detection is done in-fiber[1]. Easily extendable to a complete in-fiber setup by replacing the free-space photodiode for a fiber-coupled detector, the design is very compact, doesn't need any alignment and has a high degree of scalability. Because FAOMs work in the Bragg regime, here we don't make use of the 0th and ±1st orders as in the conventional approach. Light coming out from the FAOM is always the 1st order diffraction and hence this light will always pick up a shift Δ independently of the direction of propagation. As a result (this is explained in the following paragraphs), the beat note comes at a frequency 2Δ.

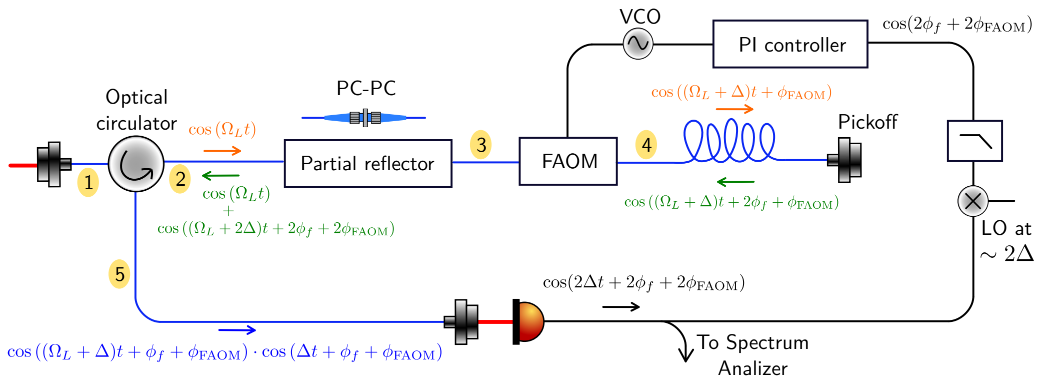

Figure 10: Experimental setup for the all in-fiber FNC. The coupled light double-passes the FAOM and the long fiber used to deliver light to another site. This light gets frequency-shifted 2Δ, twice the driving frequency of the FAOM, and gains a phase $2(\phi_{\text{FAOM}} + \phi_f)$. The interference with the reflected light in the *Partial reflector* (made of a PC to PC fiber connection) produces a beat note at 2Δ that is detected at the photodiode. With the PLL, the FAOM is driven such that ϕ_{FAOM} cancels out the phase noise ϕ_{f} induced by the fiber.

The experimental setup for the in-fiber and stable light transfer is shown in Figure 10. The stable beam at 729 nm is coupled into a fiber and sent to an optical circulator. The light travelling forward (to the right and in orange in the schematics) passes through a partial reflector, a FAOM and travels all the way through a long fiber terminated with a FC/PC connection. This type of termination has a glass-to-air back-reflection of $\sim 4\%$ or -14 dB. Before the reflection, the signal is $\cos((\Omega_L+\Delta)t+\phi_{\text{FAOM}}+\phi_f)$. In the return path the light experiences the same perturbations due to the fibers and the FAOM and arrives at the partial reflector as $\cos((\Omega_L+2\Delta)t+2\phi_{\text{FAOM}}+2\phi_f)$. There it interferes with the initially reflected signal $\cos(\Omega_L t)$ producing a beat note at around 2Δ, twice the FAOM's modulation frequency. This beat note is detected by the photodiode (that also acts as a low-pass filter for the optical frequencies) and sent to a PLL. The mixer with the local oscillator at 2Δ down-converts the signal to DC and with the locked-loop, the FAOM is modulated so as to compensate for the phase noise ($\phi_{\text{FAOM}} = -\phi_f$) and the fiber noise is suppressed.

Here, a PC to PC fiber connection made with two APC to PC fibers is used as a partial reflector. This type of connection has a return loss of approximately -30 dB or 0.1%, this is relatively small but enough to create a beat note. If more back reflection is needed or/and to minimise the losses in the connections, an in-line fiber partial reflector could alternatively be used.

[1]The original idea is from Maciej Malinowski, a PhD student in the TIQI group.

3.2.1 Characterization of the optical circulator

The circulator used in the setup is a 3-port, single-mode and non polarization-maintaining optical circulator from Ascentta (model: VCIR-3-729-S-L-10-FA). The device has a nominal Insertion Loss in all polarization states and directions of 1.8 dB and a Polarization Dependent Loss (PDL) of 0.2 dB. The instability of the amplitude of the beat note in the first attempts of the all in-fiber FNC motivated the characterization of the circulator and the dependence of its performance on polarization.

To measure the effect of polarization, we measured the transmission of the circulator while scanning all polarization directions of the input light. To do so, a $\lambda/2$ waveplate was placed in the free-space beam before coupling into the fiber. The table in Figure 11 shows the maximum and minimum transmitted power in the two transmission directions ($1 \rightarrow 2$ and $2 \rightarrow 3$) as well as their Insertion Loss (IL) and polarization-dependent loss (PDL). From the measurements we conclude that while for the $1 \rightarrow 2$ direction, IL and PDL fall under the manufacturer's specifications, this is not the case for the reverse direction ($2 \rightarrow 3$) that has a greater PDL and a much greater IL.

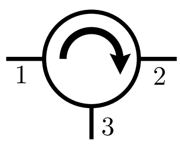

	Transmitted power	Insertion loss	PDL
$1 \rightarrow 2$	max 1.24 mW min 1.19 mW	1.2 dB	0.2 dB
$2 \rightarrow 3$	max 0.59 mW min 0.53 mW	4.6 dB	0.5 dB

Figure 11: Maximum and minimum transmitted power when scanning the direction of polarization. The measurement of $1 \rightarrow 2$ ($2 \rightarrow 3$) was taken inserting 1.60 mW from port 1 (port 2), rotating the waveplate and measuring the output power in port 2 (port 3). The insertion loss is calculated as $\mathrm{IL} = 10\log(P_{\mathrm{out}}/P_{\mathrm{in}})$, being P_{out} the mean of the transmitted power. For the PDL, we used $\mathrm{PDL} = 10\log(P_{\mathrm{max}}/P_{\mathrm{min}})$ being $P_{\mathrm{max/min}}$ the maximum and minimum transmitted powers.

3.2.2 Power attenuation

In this section, we characterize the total power attenuation of the setup as well the insertion losses of each of the sections that integrate it.

The power is measured in the setup points 1 to 5 marked with a yellow label in Figure 11. There are 1.65 mW of power that couple into the fiber. The $1 \rightarrow 2$ direction of the circulator transmits the 76% of the incoming power, arriving 1.25 mW at the partial reflector. Being made of two APC to PC fibers, up to 2.9 dB power loss is expected in this stage ($2 \cdot 0.8$ dB $= 1.6$ dB from the fibers and connections, $2 \cdot 0.5$ dB $= 1$ dB for the two APC to APC connections and up to 0.3 dB for the PC to PC connection). Experimentally, probably because of non-idealities and imperfect fiber to fiber connections, an attenuation of 3.7 dB is measured. In a first approach, after the FAOM that adds a loss of 4.4 dB, light is sent to a fiber terminated with a fiber optic retroreflector (FOR, model P5-780R-P01-1 from Thorlabs) that reflects the light back and that has a typical insertion loss of 2 dB. Considering that on the way back the losses are the same, we expect that an 1.15% of the incident power or 18.9 μW (calculated from an attenuation of 19.4 dB) arrive at point 2 and add up with the 1.65 μW calculated to be directly reflected in the initial partial reflector. This is a total of 20.6 μW at port 2 of the circulator. Using the characterized insertion loss for the $2 \rightarrow 3$ direction of the circulator (see Section 3.2.1), we expect to measure 7.1 μW at terminal 3. This differs by just some μW with respect to the 10.4 μW measured in Point 5. The slight discrepancy might be due to error propagation, imperfect accuracy, inestability of the connections or because having underestimated the power reflected in the PC to PC connection.

Setup point	Power	Element	Attenuation	Cumulative attenuation
1	1.65 mW	-	-	-
2	1.25 mW	Circulator (1-2)	1.2 dB	1.2 dB
3	0.53 mW	Partial reflector	3.7 dB	4.9 dB
4	0.19 mW	FAOM	4.4 dB	9.3 dB
4 (return)	-	FOR	2 dB	11.3 dB
2 (return)	-	FAOM + PR	8.1 dB	19.4 dB
5	10.4 μW	Circulator (2-3)	4.6 dB	22 dB

Table 1: Power attenuation along the setup terminated with a Fiber Optic Retroreflector. In each of the measurement points (indicated in 10) the power is measured. The measurements are used to calculate the insertion loss of each element.

After that, for a realistic approach of light delivery, once we knew that we had enough power to see a beat note and lock it, we replaced the retroreflector for a PC-terminated fiber that did allow for light delivery. With that, from 1.58 mW of coupled-in power, 0.132 mW or 8.4% (attenuation of 10.8 dB) were delivered to the end fiber end, while just 0.75 μW (0.05%) were reflected back to port 3 creating a beat note and using it to lock the setup. Despite being a very small fraction of the incoming light, the power was enough for FNC (the amplitude of the beatnote measured with the spectrum analyzer was of -72dBm).

3.2.3 Beat note signal

In the initial efforts, the amplitude of the beat note amplitude suffered from strong oscillations in amplitude that made locking almost impossible. By measuring an almost constant power at the circulator's port-3 (point 5 in Figure 10) we discarded power fluctuations to be the origin of the problem. The issue could also have roots in the polarization sensitivity. Despite having measured a low PDL for the optical circulator and being the FAOM not typically very sensitive to polarization (typical PDL of 0.5 dB), these devices are just single mode and not polarization-maintaining. The change of polarization in them could possibly affect the interference measured in the photodiode. With this hypothesis in mind, we decided to add an In-Line Fiber Optic Polarization Controller (CPC900 from Thorlabs) before the FAOM with the purpose of handling the polarization. With the addition and proper adjustment of the polarization controller, we could reduce the fluctuation of almost 40 dB to less than 5 dB and the stability of the locked signal increased significantly.

The beat note spectrum at the photodiode is shown in Figure 12. The carrier peak appears at $\sim$ 300 MHz, twice the driving frequency of the FAOM. Because of the fiber losses, it has a quite small but sufficient for locking amplitude of ~ -70 dB (measured in the realistic set-up with an AC/PC fiber). When directly driven by an external source, some acoustic noise of a few kHz and approximately 10 dB above the noise floor was present. This noise was effectively suppressed when locking the PLL. Starting with a narrow beat note with a width at FWHM of $\sim$ 20 Hz, with the feedback loop we manage to shrink it even more, down to less than 5 Hz. It is worth mentioning that in this case we took the measurements with another spectrometer that has a higher resolution of 1 Hz. For the previous measurements presented, the highest resolution of the spectrometer used is 10 Hz and this probably prevented us from seeing the decrease of the line-width when locking and probably also avoided us from seeing finer details of the spectra.

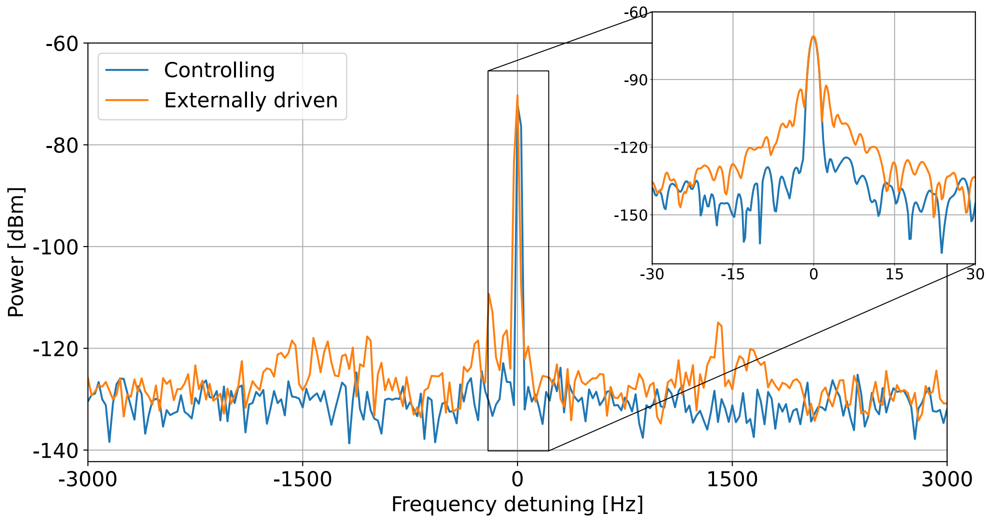

Figure 12: Beat notes of the all in-fiber FNC when locking the FAOM (blue spectrum, centered at 299.99997 MHz) and when driving the FAOM directly with the LO (orange spectrum, centered at 300.00018 MHz). The offset $\sim$ 10 dB above the noise floor and $\sim$ 4 KHz wide in the orange trace disappears when locking the setup. The inset plot, taken with a resolution of 1 Hz, clearly shows the the reduction of linewidth when using the PLL.

3.3 All in-fiber scalable FNC

Having presented a new method for FNC to scale the noise cancellation to several fibers using just one setup and also a new all in-fiber approach to the conventional FNC, the next reasonable step would be a scalable and all in-fiber setup that integrates both. Such setup is power-efficient, easily scalable and all in-fiber. It is shown in the diagram in Figure 13. The laser setup is located in *Table 1* and a pair of fibers deliver its light to *Table 2*, where the experiment would sit. The FNC setup in *Table 1* cleans the phase noise induced by the fiber *Fiber 1* and in this way the light arriving to *Table 2* through this fiber is free from phase noise and serves as the reference for the second FNC. This second setup is in *Table 2* and suppresses the noise induced by the fiber *Fiber 1* and the symmetric paths after splitting. With this technique we would be able to deliver narrow linewidth light from one location to another and also split this light into several beams without causing broadening to the spectrum just using two control loops and without using free space.

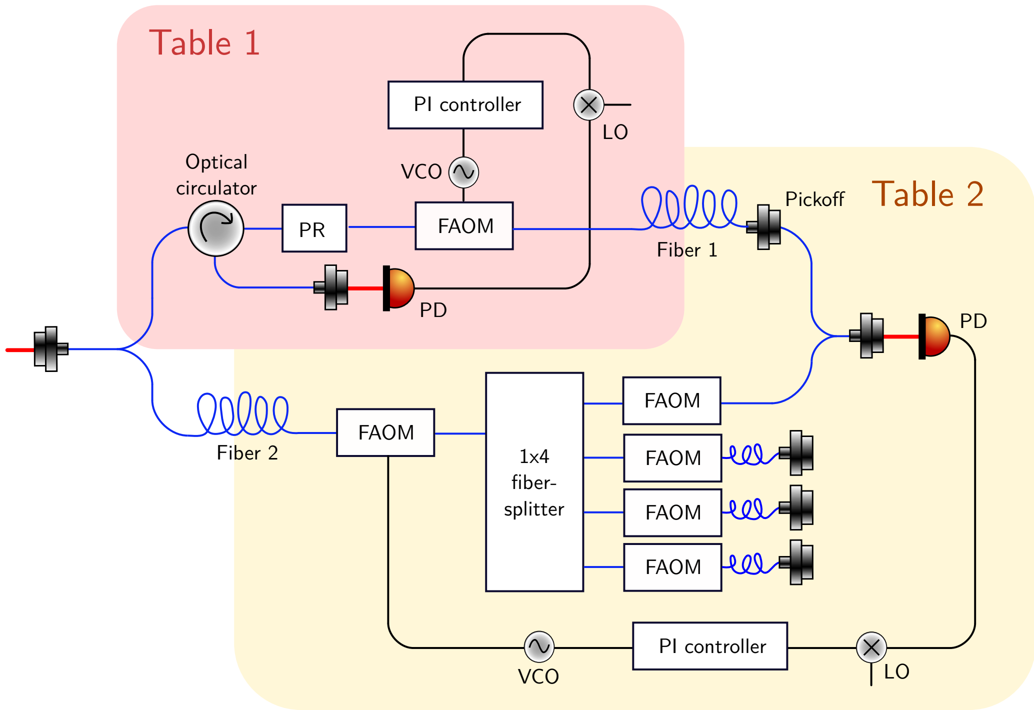

Figure 13: Complete all in-fiber FNC. Two fibers are used to deliver the light from the laser's table (*Table 1*) to the experiment's table (*Table 2*). In *Table 1* a full in-fiber FNC setup supresses the noise added by *Fiber 1*, used to bring a clean reference to *Table 2*. *Fiber 2* delivers the light that will be used for the experiment. After splitting into four signals, one of the outputs is used to cancel the phase noise induced by *Fiber 2* and the rest of fibers in *Table 2*. Being the fibers after splitting placed in a compact way, phase noise would be common among all them and FNC will not only correct for the noise in *Fiber 2* but also for the one produced after the splitter.

4 Outlook

In this part of the project we built and tested two setups for new approaches to fiber noise cancellation that allow for more compact, power-efficient and scalable setups. We described, built and tested an scalable beat-note lock in which one feedback loop is used to control phase noise in several fibers. With these tests we saw that the various paths did not exhibit differential noise. This made possible the suppression of noise in all the paths by just controlling one. In turn, the noise cancellation validates the assumption of the common mode noise. It is worth noting, however, that this assumption could eventually break down if the paths are not kept as identical as possible, if they are too long or pick up too much noise.

Besides, we also built and characterized an all in-fiber method for the noise cancellation and proposed a design that integrates the two presented methods that would enable for a all in-fiber and efficient setup for stable light delivery.

Part II

Simmulations of an Isospaced ion string with Mixed-Spieces

5 Introduction

One of the proposed approaches to scale up ion trap quantum computing for near term applications such as NISQ type devices is to use long ion strings in a Paul trap. While this approach of having long string of ions in a single potential well simplifies the design of the trap and also the voltage control of the electrodes -it doesn't require several trapping regions and transport or splitting routines- it presents bigger constraints on the individual addressing of qubits. To overcome this, one of the proposed solutions are glass written waveguides, where each core is imaged to a single ion. To ease the manufacturing of these devices, equal spacing of ions is desirable and a way to achieve this geometry is to use an anharmonic term that counteracts the Coulomb interaction that is one of the causes of the typical non-equally spaced distribution.

In this part we present the calculation of the equilibrium positions and normal modes of motion of a mixed-spieces linear string of ions under an *isospaced* potential that keeps them uniformly spaced. The first part includes a brief introduction to linear Paul traps and motivates the usage of mixed-spices and anharmonic potentials. Then we present the analytical derivation of the isospaced potential and the general derivation of the normal modes of a mixed string. Finally, we explain the method used and show the results of the calculations of the normal modes.

5.1 Paul traps

The classical laws of electromagnetism predict that it is impossible to confine a charged particle using a static potential. This is known as the Earnshaw's theorem and as has the consequence that without a combination of electric and magnetic fields or without time-dependent fields it is impossible to confine ions. Different trap solutions that overcome the issue have historically been implemented: Penning traps that use both electric and magnetic fields and Paul traps that use an RF electric field.

In a Paul trap, a combination of DC and RF feilds are used to generate a quadrupole potential along two axes - commonly referred to as the radial directions - while purely DC fileds are used to confined the ions along a third direction - the axial direction. Normally, the DC confinement is weaker than the radial, allowing the creation of linear strings.

More specifically, the DC field creates a static potential [12] well described by

$$U_S = \frac{1}{2} m \omega_z^2 \left(z^2 - \frac{x^2 + y^2}{2} \right) \quad \text{with} \quad \omega_z = \sqrt{\frac{2\kappa Z e U_0}{m}} \tag{4}$$

where Ze is the charge of the ion, κ is a geometrical factor, U_0 is the voltage applied and m is the mass of the ion. Without an extra oscillating field in the perpendicular plane, the ions would be anti-confined as a result of Poisson's law. An RF quadrupole potential in this plane counteracts for this effect and keeps the ions dynamically localized. A typical implementation consists of four rod-shaped electrodes that periodically alternate the sign of the potential so that the accelerated ions change direction continuously avoiding any collision with the electrodes. The movement is described by Mathieu equations and consists of a rapid oscillation known as micro-motion superposed with a secular motion [13]. If micromotion is averaged, the secular motion can be approximated by an harmonic oscillation at a secular frequency $\omega_{sec/x,y,z}$ that depends on the mass and charge of the ion [14]. On average, the ion behaves as it was trapped radially in an quadratic potential, also called pseudo-potential, given by

$$U_{RF} = \frac{1}{2}m(\omega_x x^2 + \omega_y y^2) \quad \text{with} \quad \omega_{x,y} = \frac{ZeV_{RF,x/y}}{\sqrt{2}m\Omega_{RF}R^2} \tag{5}$$

The secular frequency is of the order of some MHz and $V_{RF,x/y}$ is the voltage applied to diagonally opposite electrodes, Ω_{RF} is the frequency of oscillation of the field and R is the radius of the trap. Figure 14 shows a typical implementation of these potentials.

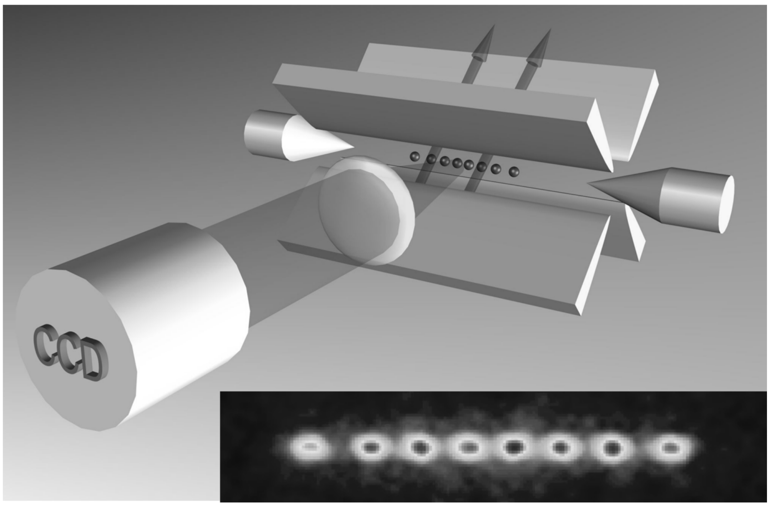

Figure 14: Linear Paul trap with a string of ions. The four blades oscillate at high voltages at RF frequencies and provide radial confinement while the two needle electrodes create the DC field. The picture was extracted from [15].

5.1.1 Collective oscillations

Coulomb coupling is key when it comes to conventional quantum gates. The strong interactions between the ions make them oscillate collectively in a set of non-degenerate normal modes that can be addressed with a laser. This way the collective vibration is used as a quantum bus to couple ions. In linear traps, we can usually distinguish between axial modes - along the z direction in this report - and radial modes - in the xy plane. In a string of N ions, there are $3N$ modes. Figure 15 shows, shows the normal mode of motion for a chain of 2 and 3 ions.

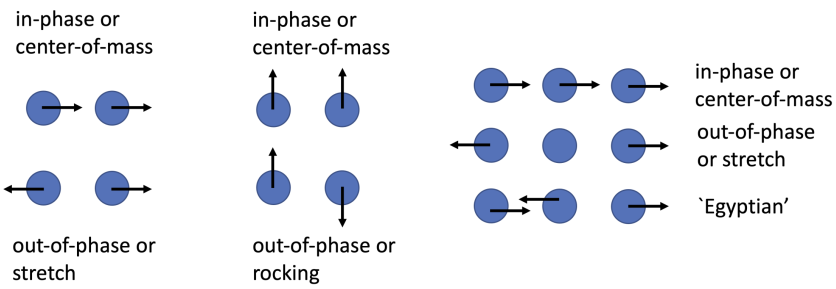

Figure 15: Normal modes of motion of a chain of 2 ions (left and middle) and 3 ions (right).

The mode with lowest energy is the COM mode and is characterized by all the ions moving together back and forth [12]. This oscillation comes at a frequency ω_z. In order to keep a linear string and avoid the transition to other configurations, the COM frequency ω_z needs to be much smaller than $\omega_{x/y}$. Also the COM mode is the one that gets heated more easily, because ions move in phase and all of them couple to the noise. On the other hand, out-of-phase modes don't heat up that much because the movement on opposite directions cancels out any coupling to a constant stray field and a field with a gradient is needed to couple to the noise.

5.1.2 Mixed-species ion string

Trapped ion strings need to be cooled down to almost the ground state of motion for high-fidelity gates. The cooling of ions can be done by means of laser-cooling and using Coulomb interactions it is possible to propagate the cooling to an entire string. The process is known as *Sympathetic cooling* and requires close proximity between the ions being sympathetically cooled and the *coolans*. The short distances required present a problem when the cooling is applied to chain of identical ions: the large amount of scattered photons are easily absorbed by neighbouring ions causing information loss and decoherence. One solution that overcomes the problem is the combination of different ion species: one specie to store information and the other to cool. This way the scattered photons are unlikely to be absorbed by the data ions since they are far-detunned from any transition in them.

When adding new species to the chain, the modes of oscillation change and the characteristics of the new oscillations depend on the relative masses of the ion and the symmetries of the chain. When it comes to the radial motion, ions of different masses tend to move almost independently and no collective motion is observed. This doesn't happen in the case of identical masses and has roots mass-dependent pseudo-potential confinement.

5.1.3 Linear string

In a linear Paul trap, the outer ions push inner ions togheter leading to a non-uniform spacing. Usually the separation is of several μm. As said, typically the external potential is harmonic in the three spacial directions with strong confinement in the radial plane ($\omega_x, \omega_y \gg \omega_z$). However, an harmonic axial potential presents some issues when adding more ions to the chain. It has non homogeneous equilibrium positions thet tend to be closer at the center of the string and more separated at the edges. If an equally spaced ion chain is desired, anharmonicities to the external potential can be added so as to compensate for Coulomb interactions.

5.2 Potential for an isospaced ion string

The conventional way to extract the equilibrium positions and phonon modes of ions in a linear trap is through the minimization of the system's potential V and diagonalization of the Hamiltonian H_0 that describes the motion of the ions [16]. If a particular arrangement of the ions is desired, the reverse problem has to be solved. In other words, the external potential that results in a desired distribution is unknown. Though an analytical solution doesn't always exist, few distributions as a string of equidistant ions have one. In the following paragraphs we summarize the key steps of the analytical derivation of the isospaced potential that is presented in [17].

The potential of a string with equally spaced ions has two contributions, one coming from the external trapping potential and the other that is due to Coulomb interactions between the ions

$$V(\vec{r}_i) = V_{ext}(\vec{r}_i) + \sum_{i \neq j} \frac{e}{4\pi\epsilon_0 |\vec{r}_i - \vec{r}_j|} = V_{ext}(\vec{r}_i) + \sum_{i \neq j} \frac{e}{4\pi\epsilon_0 |\vec{r}_i - \vec{r}_j|} \tag{6}$$

If the crystal is a string of N ions equally separated a distance d and oriented along the z direction, the i-th ion experiences an electrostatic field pointing also in z direction that can be expressed as

$$E(\vec{r}_i) = \sum_{i \neq j} \frac{e}{4\pi\epsilon_0 |\vec{r}_i - \vec{r}_j|^2} = \frac{e}{4\pi\epsilon_0 d^2} \left(\sum_{n=0}^{i-1} \frac{1}{n^2} + \sum_{n=i+1}^{N} \frac{1}{n^2} \right) \equiv E_i \tag{7}$$

Defining $E_{nn} = e/4\pi\epsilon_0 d^2$ as the field strength created by a nearest-neighbour ion and making use of polygamma functions, the expression can be rewritten as

$$E_i = E_{nn} \left(\psi^{(1)}(N - i + 1) - \psi^{(1)}(i) \right) \tag{8}$$

The field created by the external potential V_{ext} has to contrarest the effect of the Coulomb repulsion in each of the ions' positions but not in between. This means that it has to fulfil

$$E_{ext} = -\frac{dV_{ext}}{dz}\bigg|_{z=i\cdot d} = -E_i \tag{9}$$

Integrating the last expression and setting the origin of potential at $z = 0$, the potential is

$$V_{ext,z} = V_0 - E_{nn} d \left(\psi^{(0)}(\tilde{z}_+) + \psi^{(0)}(\tilde{z}_-) \right) \tag{10}$$

with

$$V_0 = 2E_{nn} d\psi^{(0)}(N_+), \qquad \tilde{z}_\pm = N_+ \pm \frac{z}{d}, \qquad N_+ = \frac{N+1}{2} \tag{11}$$

In a linear trap, the ions are usually bounded radially by an effective harmonic potential (the ion i with mass m_i moves at a secular frequency $\omega_{x/y,i}$). If in z direction V_{ext} keeps them equally spaced, the potential for an N-ions linear and equally spaced string is

$$V_N(x, y, z) = V_{ext}(z) + \sum_{i=1}^{N} \frac{1}{2} m_i (\omega_{x,i}^2 x^2 + \omega_{y,i}^2 y^2) \tag{12}$$

5.3 Equilibrium positions and string dynamics

5.3.1 Equilibrium positions

The equilibrium positions can be extracted by finding the $(x, y, z)^*$ points that solve

$$\nabla(V_N + V_{\text{Coulomb}})|_{(x,y,z)^*} = 0 \tag{13}$$

Because V_N was constructed to have N equally-spaced equilibrium positions along the z direction, these equilibrium points do cancel the gradient of V_N. It is worth pointing out that the mass of the ions doesn't play any role in the equilibrium positions and hence these equilibrium positions will not change when using mixed-species ion chains - as long as all of them have the same charge.

5.3.2 Normal modes of motion

The normal modes of motion can be extracted by formulating and solving the Lagrange equations of the system [18]. Being $\{\xi_i\}_{i=1}^{3N}$ the position coordinates of the system, the kinetic and potential energies around the equilibrium positions are

$$T = \sum_{i=1}^{N} \frac{1}{2} m_i (\dot{x}_i^2 + \dot{y}_i^2 + \dot{z}_i^2) = \sum_{i=1}^{3N} \frac{1}{2} m_i \dot{\xi}_i^2 \tag{14}$$

$$U = -V_N + \sum_{i=1}^{N} \sum_{j=1}^{N} \frac{1}{4\pi\epsilon_0} \frac{e^2}{|\vec{r}_i - \vec{r}_j|^2} \simeq U_0 + \sum_{i,j=1}^{3N} \frac{\partial^2 U}{\partial \xi_i \partial \xi_j} (\xi_i - \xi_i^0)(\xi_j - \xi_j^0) \tag{15}$$

Introducing the mass weighted coordinates $\tilde{\xi}_i = \sqrt{m_i}(\xi_i - \xi_i^0)$ the expressions simplify and become analogous to the ones corresponding to the identical mass ion string. In this case the Lagrangian is

$$\mathcal{L} = T - U = \sum_{i=1}^{3N} \frac{1}{2} \dot{\tilde{\xi}}_i^2 - \sum_{i,j=1}^{3N} \frac{1}{\sqrt{m_i m_j}} \frac{\partial^2 U}{\partial \tilde{\xi}_i \partial \tilde{\xi}_j} \tilde{\xi}_i \tilde{\xi}_j \tag{16}$$

And the equation of motion for the ith ion writes

$$\frac{d}{dt} \frac{\partial \mathcal{L}}{\partial \dot{\tilde{\xi}}_i} = \frac{\partial \mathcal{L}}{\partial \tilde{\xi}_i} \implies \ddot{\tilde{\xi}}_i = \sum_{j=1}^{3N} \frac{1}{\sqrt{m_i m_j}} \frac{\partial^2 U}{\partial \tilde{\xi}_i \partial \tilde{\xi}_j} \tilde{\xi}_j \tag{17}$$

Then the normal modes of motion and their frequencies are given by the eigenvectors and eigenvalues of the Hessian matrix defined by the potential energy

$$H_{ik} = \frac{1}{\sqrt{m_i m_j}} \frac{\partial^2 U}{\partial \tilde{\xi}_i \partial \tilde{\xi}_j} \tag{18}$$

The eigenvectors $\{\tilde{e}_{\alpha,i}\}$ contain the information of the participation of each coordinate in a mode or, in other words, how much an ion moves in a particular direction with respect to the others. On the other hand, the frequency associated with each motional mode is given by $\omega_\alpha = \sqrt{\lambda_\alpha}$, with λ_α being the eigenvalue of the mode.

6 Statics and dynamics of an isospaced ion string

6.1 Method

To calculate the normal modes we use the IonSim package in Python that was developed in the group and that can be found in `https://gitlab.phys.ethz.ch/graum/ion_sim`. The package allows the calculation of the equilibrium positions, normal modes and the simulation of the dynamics of the string adding for example some damping.

We consider a long chain of $N = 11$ $^{40}Ca^+$ ions in a linear Paul trap. The confinement in the radial directions (x and y) is harmonic with a secular frequency of 2.4 MHz in both directions. In z direction we use either the isospaced potential in Equation 10 or a 6th order approximation of it. These potentials are plotted in Figure 16.

When using mixed-species, the secular frequencies that each ion experiments will depend on its mass according to Equation 4. If $^{40}Ca^+$ is subject to a secular frequency $\omega_{\text{sec},40} = 2.4$ MHz, $^{44}Ca^+$ will experiment $\omega_{\text{sec},44} = 2.4\sqrt{44/40}$ MHz $= 2.52$ MHz.

6.2 Equilibrium positions

The equilibrium positions of the ions are calculated by minimizing the potential energy according to Equation 13. Figure 16 presents the computed equilibrium positions of the chain of 11 ions for three different potentials: harmonic potential, isospaced and a 6th order approximation. The isospaced potential results in a equally spaced chain (this we verified by calculating the standard deviation of distance between ions, which is zero). The 6th order expansion results in almost the same configuration: the maximum deviation with respect of the ideal position is of just 0.26 μm and the distribution has an associated standard deviation of the order of 10^{-9} μm. In contrast, the std for the harmonic potential is of the order of 0.1 μm, indicating a non equally spaced string.

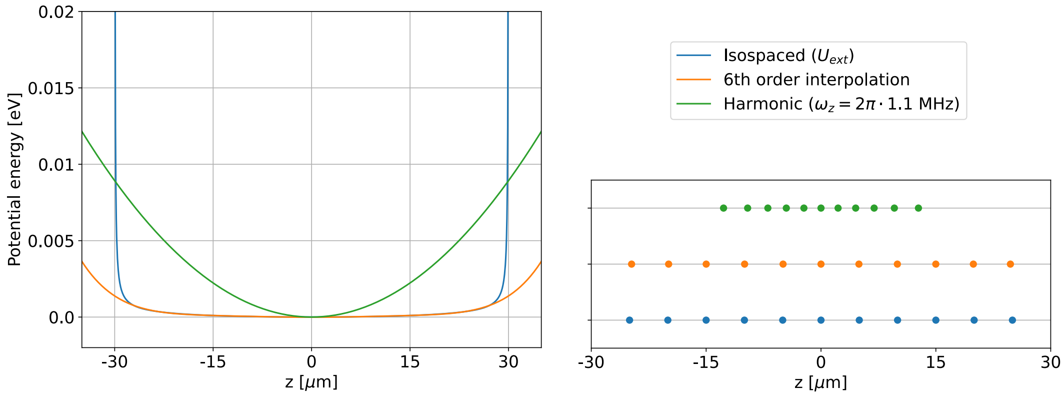

Figure 16: Left: plot of different axial potentials (linear, isospaced for 11 ions and 6th order approximation of the isospaced potential). Right: For each potential the equilibrium positions are computed.

6.3 String dynamics of 1 configuration

6.3.1 Validation

To test a proper implementation of the code to calculate normal modes in a mixed-species string, we first used it to calculate the normal modes of a berillium-magnesium ion chain in a Paul trap with quadratic potential in z direction. The secular frequencies used for the single berillium are $[\omega_x, \omega_y, \omega_z] = 2\pi \cdot [12.26, 11.19, 2.69]$ MHz and for the magnesium $[\omega_x, \omega_y, \omega_z] = 2\pi \cdot [3.72, 4.82, 1.65]$ MHz. The eigenfrequencies and the normalized eigenvectors are shown in Table 2 and coincide with the calculations presented in [19]. Figure 17 shows plots of the displacements in axial and radial direction for each of the eigenmodes.

Mode	Frequency [MHz]	$^{9}Be^{+}$	$^{24}Mg^{+}$
Radial (x)	12.1	1	0.02
	3.52	-0.02	1
Radial (y)	11.0	1	0.02
	4.67	-0.02	1
Axial (z)	4.04	0.93	-0.38
	1.90	-0.38	0.93

Table 2: Normal modes of motion for a $^{9}Be^{+}$ - $^{24}Mg^{+}$ ion string. Each mode has associated an axial or radial direction of movement and the second last columns show the relative displacement of each ion in the mode. The modes were calculated with the code and with the same data as in [19]. Obtaining the same results is a validation of a correct implementation.

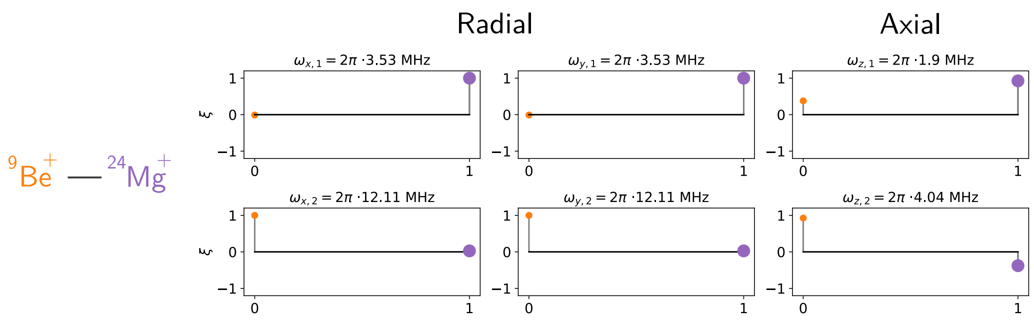

Figure 17: Normal modes of motion of a berillium-magnesium ion chain. In the radial modes, one ion oscillates while the other is almost at rest. In the axial modes both ions oscillate.

6.3.2 Normal modes of the isospaced string

Then we proceeded to the calculation of the normal modes for the longer string of 11 ions under the isospaced potential. First we started with an homogeneous chain of $^{40}Ca^{+}$ ions. The resulting axial and radial displacements for the two lowest ($\omega_{z,0}$ and $\omega_{z,1}$) and highest ($\omega_{z,0}$ and $\omega_{z,10}$) frequency modes are plotted in Figure 18. For example, we observe that for the low energy modes the collective oscillation happens in the axial direction and the out-of-phase happens in the radial while the inverse behaviour occurs for the higher frequency modes.

6.4 Comparison between configurations

Once we calculated the normal modes for a long and homogeneous isospaced chain, we analyzed how they were affected by changing the ideal isospaced potential for a polynomial approximation (practically implementable) and by replacing some of the ions for other species with different mass. The comparison is done by plotting the difference in the displacement of the ions for the various modes and the difference of frequency of each mode.

6.4.1 Polynomial approximation

Figure 19 shows how the radial modes change when the analytical isospaced potential is replaced by a 6th order polynomial approximation. For each mode the difference in the displacement of each ion is plotted in color scale from dark blue (no difference) to red (the most different) in the left plot. The right plot shows the difference in frequency. We observe that the low frequency modes are the most affected both in terms of displacement and frequency. These differences are nevertheless not very strong. The ions that get differently more displaced are oscillating in both potentials and the differences in frequency are of tenths of kHz in eigenfrequencies in the MHz range.

6.5 Adding another ion species

The addition of an ion with different mass also affects the normal modes of motion. In the first comparison we change the middle $^{40}Ca^{+}$ for a $^{44}Ca^{+}$. A shift of the radial frequency is observed in all the modes. This shift is larger for the low frequency modes and in general the odd modes are less affected. Regarding the displacements, the odd modes are almost non-perturbed by the

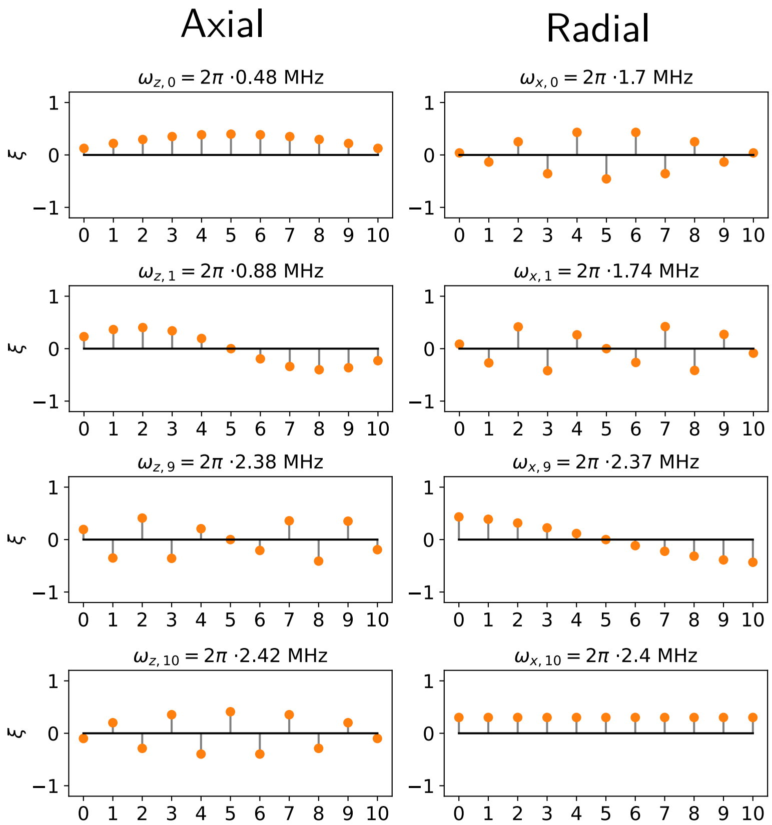

Figure 18: String dynamics in the axial and radial direction for the two eigenmodes with the lowest and highest frequency under the isospaced potential. The string consists of 11 $^{40}Ca^{+}$ ions with secular frequency in the radial direction of 2.4 MHz.

presence of a more massive ion in the middle of the chain. We can explain this by recalling that the center ion remains fixed for the odd modes, and thus its role in these modes in not very relevant. For the even modes, in which the middle ion does move, the center ions change more their amplitude of oscillation since they are more affected by the presence of a $^{44}Ca^{+}$ in the center.

If instead of just the middle ion, the three middle ions are replaced for $^{44}Ca^{+}$, more noticeable changes in all the modes occur. Figure 21 shows the difference in the displacement and frequency of the modes of such chain under the 6th order potential with respect to the homogeneous case with the analytical isospaced potential. Again, the low frequency modes are the ones that shift more in frequency but here we don't observe the parity pattern seen before. The addition of more massive ions in positions 4th and 6th alter much more the dynamics of the chain (before just the ion in the highly symmetrical 5th position was changed).

For completeness, in Figure 22 we present plots of the axial and radial displacements together with their frequencies for the two lowest and two highest frequency modes for the string with 3 $^{44}Ca^{+}$ ions under the 6th order polynomial approximation. Comparing with Figure 18, we conclude again that the dynamics are appreciably affected despite they follow the same trend. Moreover, now we can also infer that the replacement of the 3 ions in the middle for $^{44}Ca^{+}$ is what contributes the most to the change and not using an approximation of the potential.

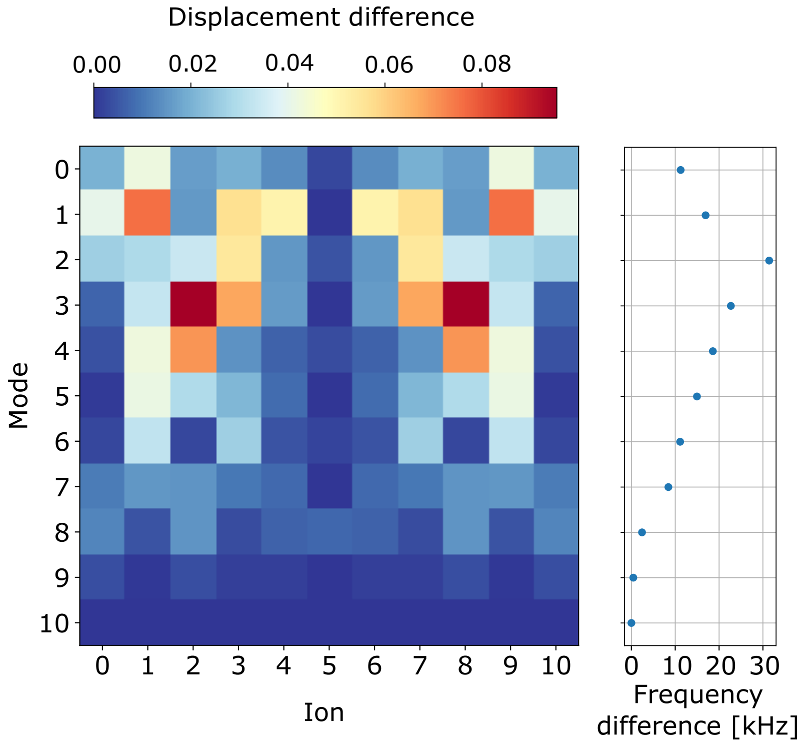

Figure 19: Comparison of the radial modes of a chain of 11 $^{40}Ca^{+}$ ions under the analytical isospaced potential versus its sixth order polynomial approximation. The left color plot shows the difference in displacement for each mode and ion and the plot in the right shows the difference in frequency of the modes.

7 Outlook

In this second part we explored the static and dynamical behaviour of a string of ions under a potential constructed to keep the ions equally spaced. We reviewed of the derivation of such potential and proceeded with the calculation of its equilibrium positions and normal modes of motion. To study an implementable scenario, we approximated the analytical potential for a 6th order polynomial and showed that both the equilibrium position and the normal modes are essentially the same. Then we extended the calculations to mixed-species strings of ions, argued the invariance of the equilibrium positions and studied how a mixed-spicies chain produced more notable changes in the normal modes.

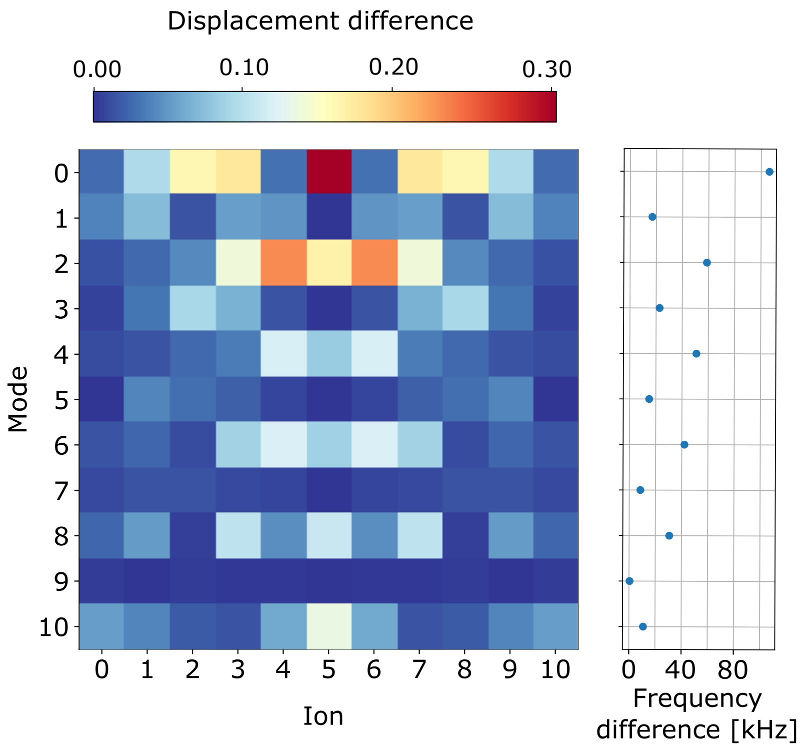

Figure 20: Comparison of the radial modes of a chain of 10 $^{40}Ca^{+}$ ions with 1 $^{44}Ca^{+}$ in the middle (total of 11 ions) under the 6th order polynomial approximation (the comparison is done with respect to the homogeneous chain under the analytical isospaced potential). The color in the 2D plot indicates the difference in displacement for each mode and ion and the plot in the right shows the difference of the frequency mode.

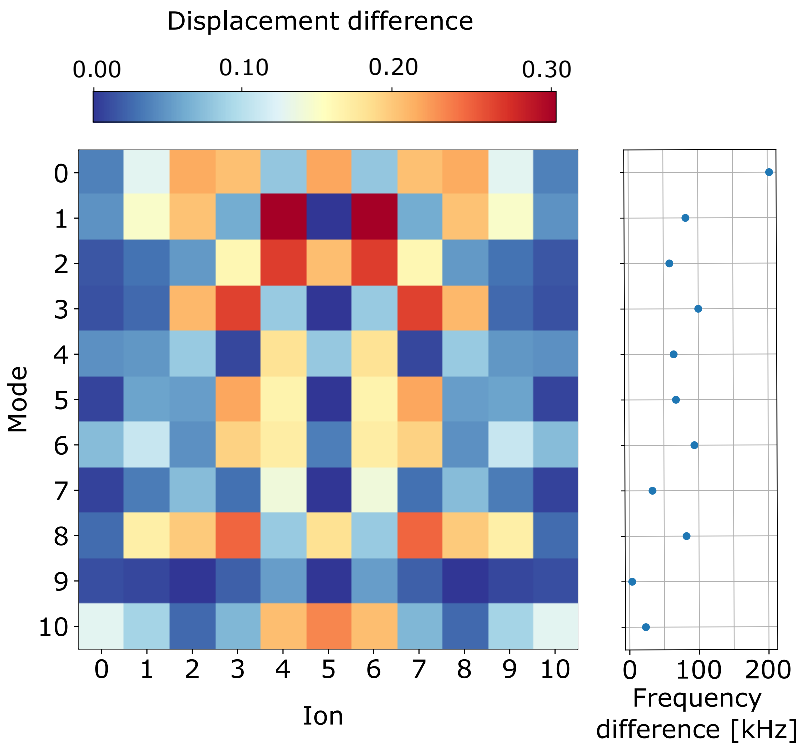

Figure 21: Comparison of the radial modes of a chain of 8 $^{40}Ca^{+}$ ions with 3 $^{44}Ca^{+}$ in the middle (total of 11 ions) under the 6th order polynomial approximation (the comparison is done with respect to the homogeneous chain under the analytical isospaced potential). The color in the 2D plot in the left indicates the difference in displacement for each mode and ion and the plot in the right shows the difference of the frequency mode.

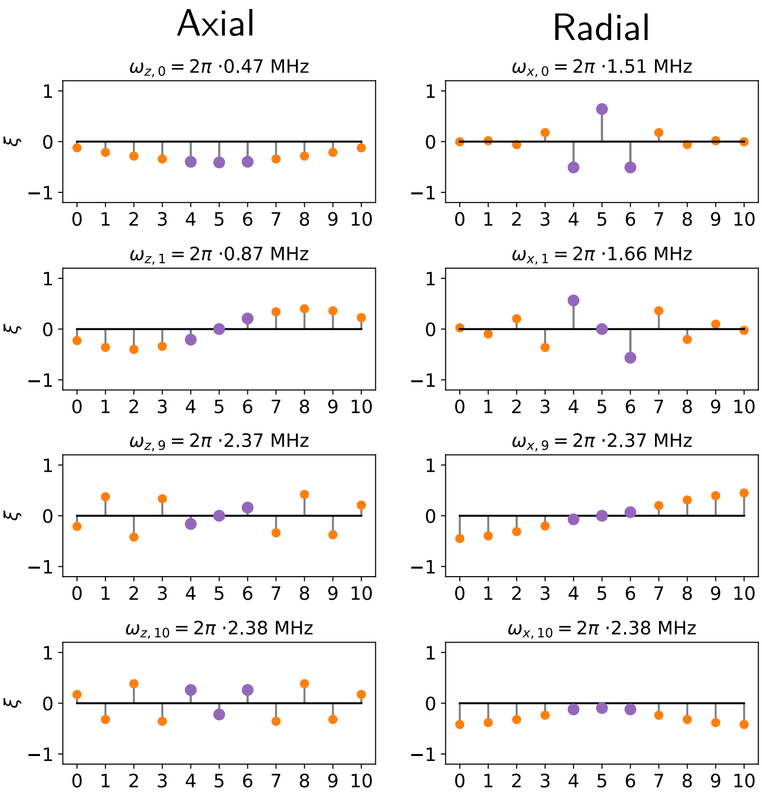

Figure 22: String dynamics in the axial and radial direction for the two eigenmodes with the lowest and highest frequency of a mixed-species ion string of 11 ions (8 $^{40}Ca^{+}$ ions with 3 $^{44}Ca^{+}$ ions in the middle) under the 6th order polynomial. approximation of the isospaced potential.

References

[1] Yi Pang, Jeffrey J. Hamilton, and Jean-Paul Richard. "Frequency noise induced by fiber perturbations in a fiber-linked stabilized laser". In: *Appl. Opt.* 31.36 (Dec. 1992), pp. 7532–7534.

[2] Long-Sheng Ma et al. "Delivering the same optical frequency at two places: accurate cancellation of phase noise introduced by an optical fiber or other time-varying path". In: *Opt. Lett.* 19.21 (Nov. 1994), pp. 1777–1779.

[3] G. B. Hocker. "Fiber-optic sensing of pressure and temperature". In: *Appl. Opt.* 18.9 (May 1979), pp. 1445–1448.

[4] A. Barlow and D. Payne. "The stress-optic effect in optical fibers". In: *IEEE Journal of Quantum Electronics* 19.5 (1983), pp. 834–839. DOI: 10.1109/JQE.1983.1071934.

[5] K. Blotekjaer. "Thermal noise in optical fibers and its influence on long-distance coherent communication systems". In: *Journal of Lightwave Technology* 10.1 (1992), pp. 36–41.

[6] Pedro Rosso. *Cancellation of phase noise induced by an optical fiber in a compact setup.* Tech. rep. ETH, Department of Physics, Mar. 2019.

[7] Edward A. Lee and David G. Messerschmitt. "Phase-Locked Loops". In: *Digital Communication.* Boston, MA: Springer US, 1994, pp. 700–724.

[8] Magnus Christie et al. "Fiber coupled acousto-optic modulators for near UV and blue wavelength applications". In: Feb. 2018, p. 18.

[9] Jia-ming Liu. "Acousto-optic devices". In: *Photonic Devices.* Cambridge University Press, 2005.

[10] Christoph Fischer. *Implementation of a Digital Lock-in Amplifier on a Field Programmable Gate Array and its Remote Control in a Local Area Network.* Tech. rep. ETH, Department of Physics, 2015.

[11] Martin Stadler. *Improving the Electronically Variable Interactive Lockbox (EVIL).* Tech. rep. ETH, Department of Physics, 2017.

[12] D.J. Wineland et al. *Experimental Issues in Coherent Quantum-State Manipulation of Trapped Atomic Ions.* 1998.

[13] Pradip K. Ghosh. In: *Ion Traps.* Oxford (United Kingdom): Clarendon Press, 1994.

[14] D. Leibfried et al. "Quantum dynamics of single trapped ions". In: *Rev. Mod. Phys.* 75 (1 Mar. 2003), pp. 281–324.

[15] Jurgen Eschner. *Quantum computation with trapped ions.* 1998.

[16] D. F. V. James. "Quantum dynamics of cold trapped ions with application to quantum computation". In: *Applied Physics B: Lasers and Optics* 66.2 (Feb. 1998), pp. 181–190.

[17] Michael Johanning. "Isospaced linear ion strings". In: *Applied Physics B: Lasers and Optics* 122, 71 (Apr. 2016), p. 71.

[18] Giovanna Morigi and H. Walther. "Two-species Coulomb chains for quantum information". In: *The European Physical Journal D* 13 (Jan. 2001), pp. 261–269.

[19] Jonathan P. Home. *Quantum science and metrology with mixed-species ion chains.* 2013.